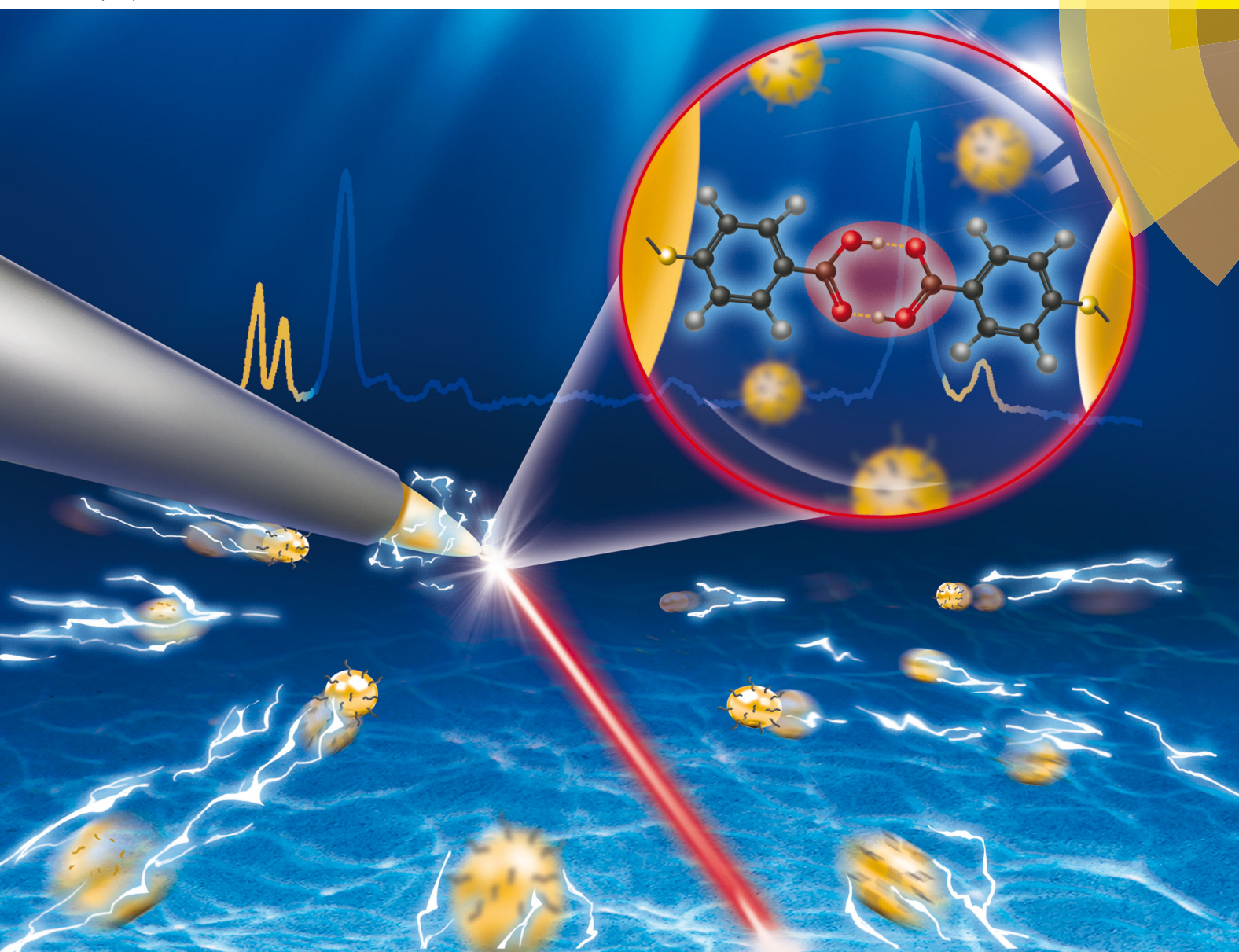
Physical Chemistry Chemical Physics rsc.li/pccp



ISSN 1463-9076



PAPER



View Article Online PAPER



Cite this: Phys. Chem. Chem. Phys., 2019, 21, 15940

Modulating and probing the dynamic intermolecular interactions in plasmonic molecule-pair junctions†

Tao Ma, ab Jing Guo, b Shuai Chang, * Xuewen Wang, b Jianghao Zhou, ab Feng Liang ** and Jin He** **

Reversible intermolecular interactions play critical roles in nature. However, it is still challenging to monitor the dynamic intermolecular interactions at the single-molecule level in aqueous solution. Here, we studied the dynamic changes of intermolecular interactions at the carboxyl/carboxyl interfaces between a pair of molecules trapped in a plasmonic nanocavity formed between a gold nanoparticle (GNP) and a gold nanoelectrode (GNE). The development of intermolecular interactions, including the appearance of hydrogen bonds (h-bonds), during and after single GNP collision events on the GNE, was monitored by time-resolved surface-enhanced Raman spectroscopy at a tens of milliseconds time resolution. Spectral fingerprints of the carboxyl group corresponding to non-specific intermolecular interactions and h-bonds are identified. Furthermore, we demonstrated that the strength of intermolecular interaction could be mechanically modulated by changing the applied bias at the GNE, which resulted in small and controllable changes in the nanogap distance. Unlike non-specific intermolecular interactions, the intermolecular h-bonds can only be formed stochastically and are more sensitive to the gap distance modulation. This report demonstrates a new approach to modulate and probe intermolecular interactions within nanogaps.

Received 11th April 2019, Accepted 14th June 2019

DOI: 10.1039/c9cp02030f

rsc.li/pccp

Introduction

The reversible assembly of biomacromolecules, e.g., nucleic acids, proteins, carbohydrates, and lipids, has inspired the investigations of non-covalent intermolecular interactions, such as van der Waals forces, metal atom coordination, π - π interactions and hydrogen bonds. These weak interactions form the foundation of molecular recognition and shape the structure of biomacromolecules in nature. Understanding of these non-covalent weak bonds is also important for applications such as drug design, self-assembly of molecule layers on metal surfaces,² and the synthesis of new functional materials.³ They have also been widely used in device fabrication^{4,5} and to

improve the sensitivity and selectivity of sensors^{6,7} and imaging techniques.^{8,9} For example, the quantum tunneling current via metal-molecule pair-metal junctions is sensitive to the dynamics of reversible intermolecular interactions, 10,11 thus providing molecular recognition capability based on tunneling current measurement. The recognition tunneling technique has been demonstrated to be highly effective for recognizing DNA, RNA, peptides, and carbohydrates at the single-molecule level. 12-15 However, characterizing the intermolecular interactions at the single-molecule level remains a challenging task.

Surface-enhanced Raman spectroscopy (SERS) has demonstrated the capability to study the dynamics of chemical reactions inside various metal-molecule-metal structures at the single-molecule level, 16 greatly improving our understanding of metal nanoparticle catalysis, 17 photocatalysis 18 and molecular electronics. 19 However, current research mainly focuses on the changes of stronger chemical bonds. The subtle intermolecular interactions in the molecular junction may significantly impact the SERS signals but have not been thoroughly investigated.²⁰ In the present study, we aim to use SERS to probe the dynamics of reversible intermolecular interactions between two molecules in a plasmonic molecule-pair junction.

Recently, we have used SERS to probe the dynamic formation of molecular junctions in 'nano-impact' electrochemical (EC)

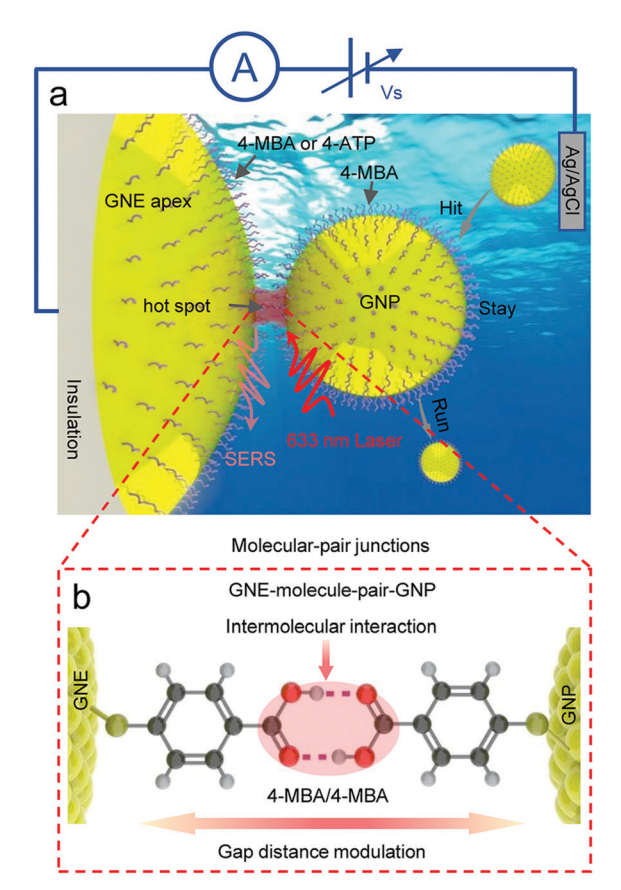
^a The State Key Laboratory of Refractories and Metallurgy, School of Chemistry and Chemical Engineering, School of Materials and Metallurgy, Wuhan University of Science and Technology, Wuhan, 430081, China. E-mail: schang23@wust.edu.cn, feng.liang@whu.edu.cn

^b Department of Physics, Florida International University, Miami, Florida 33199, USA. E-mail: jinhe@fiu.edu

^c Biomolecular Science Institute, Florida International University, Miami, Florida 33199, USA

[†] Electronic supplementary information (ESI) available: DFT calculations, SERS spectra data of 4-ATP and 4-MBA one-molecule junctions, extra SERS spectra data of pair-junctions, and current change signals. See DOI: 10.1039/c9cp02030f

PCCP Paper



Scheme 1 (a) Experimental setup and the "hit-stay-run" collision events of 40 nm diameter GNP on the apex of a partially insulated GNE by highdensity polyethylene (HDPE). The radius of the GNE apex is in the range of 100-200 nm. (b) The structure of collision formed molecule-pair junction GNE-4-MBA/4-MBA-GNP. The size is not to scale.

experiments²¹ when a gold nanoparticle (GNP) collides with a chemically modified gold nanoelectrode (GNE) (see Scheme 1a).²² 'Hotspots' with extremely high local optical fields are formed in the GNP-molecule-GNE structure, providing the opportunity to study the evolution of chemical interactions in molecular junctions during and after collision events. To form a well-defined intermolecular interface, we chemically modified surfaces of both GNE and GNP. As shown in Scheme 1a, the collision events of free-moving GNPs at the surface of GNE lead to the formation of molecule-pair junctions. A non-electroactive molecule 4-mercaptobenzoic acid (4-MBA) was chosen as the model molecule to modify the gold surface, enabling the formation of a molecule-pair, 4-MBA/4-MBA (see Scheme 1b). The vibrational modes of the carboxyl (-COOH) group of 4-MBA are very sensitive to subtle local chemical and environmental changes.²³ Therefore, the 4-MBA molecule has been extensively studied for SERS-based pH and cation ion detection methods. 24,25 For comparison, we also used 4-aminothiophenol (4-ATP) to construct a 4-ATP/4-MBA molecule pair in control experiments. When using 4-ATP, the experimental conditions are carefully monitored to avoid possible dimer formation.²⁶ The intermolecular interactions between two carboxyl groups or between carboxyl and amine groups induce the appearance and

enhancement of multiple asymmetric vibrational modes of 4-MBA. The appearances and changes of these new modes are used as sensitive probes to analyze the dynamic development and weakening of the intermolecular interactions in both dynamic and static molecule-pair junctions.

One advantage of the GNP-molecule-GNE structure is that we can perform well-controlled electromechanical modulation to the plasmonic molecular junction. Electrical and electrochemical potential dependent Raman changes have been investigated before. 27-29 However, the effect of gap distance changes induced by the applied bias has not been investigated. By applying a small bias (<1 V) at the GNE, we demonstrated that the junction distance can be slowly and slightly changed in a controlled way. The non-covalent intermolecular interactions are much weaker than the intramolecular bonds and thiol-gold bond at the molecule-gold interface; therefore must be most sensitive to the change of junction distance. We show here that we can electromechanically modulate these intermolecular interactions and probe their changes in Raman spectra. We can also separate gold-molecule interfacial interactions and intermolecular interactions based on the bias-dependent spectral changes.

Results and discussion

The dynamic formation of molecule-pair junctions by GNP collision events

We first study the transient formation of molecule-pair junctions by the 'hit-stay-run' collision events of 4-MBA modified GNPs at 4-MBA or 4-ATP modified GNEs (see the diagram in Scheme 1). The formation of a molecular junction and the evolution of intermolecular interactions are monitored by timeresolved SERS during and after the GNP collision events. The results of both types of molecule-pair junctions are similar. Here, we only show the results of the GNE-4-MBA/4-MBA-GNP symmetric molecule-pair junction. The results of the GNE-4-ATP/4-MBA-GNP asymmetric molecule-pair junction are given in the ESI,† (see Fig. S3-S5).

After adding 4-MBA modified GNPs in the solution, random and transient intensity bursts are observed in the SERS time trajectory, owing to the 'hit-stay-run' collision events at the surface of the 4-MBA modified GNE. One typical SERS time trajectory with a pronounced burst is shown in Fig. 1a with zero bias applied on the GNE. The SERS time trajectory is displayed in an intensity heat map by collecting Raman spectra continuously at 50 ms per spectrum. The transient Raman spectrum of the burst, indicated by the red arrow near 27.10 s, is shown in Fig. 1b. For comparison, the Raman spectrum of the background (at 1 s) is also shown. Two most intense peaks at 1083 cm⁻¹ and 1592 cm⁻¹ are symmetric vibrational modes 7a and 8a, due to the stretching modes of Cring-S (coupled with ring) and C_{ring}-C_{ring}, respectively. They are from the benzene rings of both 4-MBA molecules. Similar transient spectra are observed at +0.5 V bias (Fig. S4, ESI†). These transient spectra are also similar to the transient spectra of GNE-4-MBA/GNP

PCCP Paper

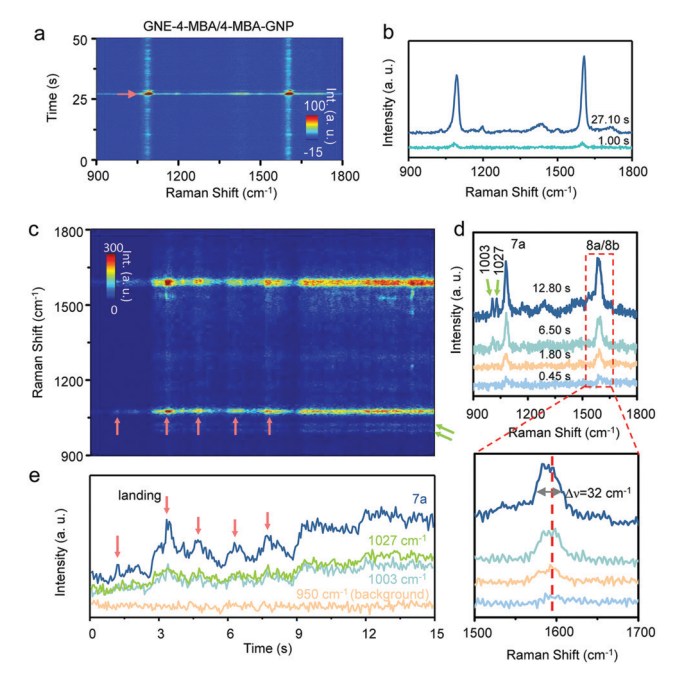


Fig. 1 Spectral changes of newly formed GNE-4-MBA/4-MBA-GNP junctions. (a) The typical SERS time trajectory in a heat map showing the transient intensity bursts induced by 'hit-stay-run' events in electrolyte. (b) A transient spectrum during a 'hit-stay-run' collision event (indicated by the pink colored arrow near 27.10 s in the trajectory in Fig. 1a) in electrolyte. The background spectrum at 1.00 s in the trajectory in Fig. 1a is also shown for comparison. (c) A typical time-resolved SERS trajectory showing the spectral changes induced by a 'hit-n-stay' event in electrolyte. (d) Four spectra appeared sequentially in trajectory (c). The zoom-in spectra at the bottom show the spectral shift of mode 8a. (e) The intensity-time traces of 1083 cm⁻¹ (7a), 1003 cm⁻¹ and 1027 cm⁻¹ and 950 cm⁻¹ (background). The results are displayed with an offset for clarity. All the results were collected with the GNE at zero bias. The electrolyte is 5 mM PBS with pH 7.4, containing 3 mM potassium ferrocyanide and 30 pM 40 nm GNPs.

one-molecule junctions at either zero or +0.5 V bias (see Fig. S3 and S4, ESI†). No new peaks due to intermolecular interaction have been observed. Therefore, the intermolecular interactions between two 4-MBA are weak and difficult to develop during the transient 'hit-stay-run' events in the electrolyte.

After the collision, most GNPs run away after a transient stay on the GNE. However, a few GNPs stay permanently on the GNE after the collision ('hit-n-stay'), forming stable molecular junctions. One example is shown in Fig. 1c. Discrete intensity changes are observed in the first 5 seconds, as indicated by the pink arrows. These Raman signal changes are reminiscent of the multi-peak electrochemical current changes observed by single GNP collision amperometry³⁰ and may reveal the bouncy landing of a GNP. Compared with the transient spectra during 'hit-stay-run' events, one major difference here is the rising of two new peaks at 1003 cm⁻¹ and 1027 cm⁻¹, following the appearance of 7a and 8a. There are two possible reasons for the appearance of both peaks. 1. The new peaks are due to the decarboxylation of 4-MBA to thiophenol (TP).31,32 In this case, the 1003 cm⁻¹ is from CCC in-plane bending (β_{CCC}) and the 1027 cm⁻¹ is from CH in-plane bending (β_{CH}). 2. The new peaks

are induced by the interactions with binding partners. They have often been observed when the carboxyl group of 4-MBA is involved in various interactions with heavy metal atom/ion, small molecules or biomolecules. We have also observed both peaks in established GNE-4-MBA/GNP onemolecule junctions (see Fig. S7a, ESI†). Both peaks are attributed to the asymmetric in-plane ring breathing modes (b2 modes) of 4-MBA (see ESI,† Section S2), which are due to the charge reorganization and structural deformation of the benzene ring during the interactions.33-35 Because TP cannot be converted back to 4-MBA under the same conditions, the reported concentration dependence of binding partners and the reversible change of the intensity of both peaks are difficult to explain by the 4-MBA decarboxylation. We found the two peaks are affected by the electrolyte and the interaction partner. They are stronger when the experiment is performed in DI water and the interaction is between 4-MBA and 4-ATP (see ESI,† S3). In addition, the changes of both peaks are also reversible. Therefore, we believe the second reason can better explain our results. Here, it is a result of interactions between two 4-MBA molecules. The appearance of both peaks indicates the non-specific intermolecular interactions, such as the carboxyl group involved van der Waals interactions.

Fig. 1d shows several snapshot spectra at different times along the trajectory in Fig. 1c. The zoom-in spectrum reveals the broadening and red shift of the mode 8a peak. Because the spectral resolution is about 2 cm⁻¹, the broad peak width of the 8a peak ($\sim 32 \text{ cm}^{-1}$ at half height) is due to the rise of 8b, which is a signature of a charge transfer mechanism and provides additional evidence for the existence of intermolecular interactions between 4-MBAs. The interactions between electron withdrawing carboxyl groups lower the electron density of the benzene ring and induce the chemical enhancement of asymmetric ring stretching mode 8b. Fig. 1e shows the intensity-time traces of 1083 cm⁻¹ (7a), 1003 cm⁻¹ and 1027 cm⁻¹. The stable intensity-time trace of the background at 950 cm⁻¹ is also shown as a reference. The intensity increases at 1003 and 1027 cm⁻¹ are clear, revealing the dynamic formation and continuous enhancement of intermolecular interactions at the early stage of GNP immobilization. The gradual increase of overall Raman intensity suggests that the nanogap distance decreases with the establishment of non-specific intermolecular interactions.

EC current changes are simultaneously recorded for some experiments utilizing the oxidation current of redox mediator ferrocyanide ion. Different from the one-molecule junctions such as GNE-4-ATP/GNP, 13 we never observe transient current changes for GNE-4-MBA/4-MBA-GNP molecule-pair junctions formed during the 'hit-stay-run' events with the GNE at +0.5 V versus Ag/AgCl reference electrode in electrolyte (see Fig. S9, ESI†). However, EC current changes are often observed during the transient changes of established junctions by adsorbed GNPs, which are triggered by the motion of surface gold atoms or the adsorbed GNP. Along with the EC current change, the intensity changes of both 1003 cm⁻¹ and 1027 cm⁻¹ peaks always appear in the simultaneously recorded Raman spectra.

Therefore, the stronger intermolecular interactions can improve the electronic coupling in the molecule-pair junction.

The dynamics of H-bonds in established molecule-pair iunctions

Now we focus on the dynamics of intermolecular interactions in established molecule-pair junctions under settled GNPs after collision events at zero bias. A representative SERS heat map trajectory for the 4-MBA/4-MBA junction is shown in Fig. 2a. In contrast to the transient spectra shown in Fig. 1 during the dynamic junction formation, these spectra from established junctions are generally quite stable. Especially, the stable and pronounced bands at 1003 cm⁻¹ and 1027 cm⁻¹ indicate the well-established intermolecular interactions in both moleculepair junctions. The attractive intermolecular interactions are mainly responsible for the retention of GNPs on the GNE.

Interestingly, in addition to the stabilized peaks, new transient peaks appear stochastically. As shown in Fig. 2a, a new peak near 1661 cm⁻¹ suddenly appears at 57 s and lasts for more than 10 seconds. The zoom-in trajectory (I) at the right side also clearly reveals the intensity and peak position drifts of this transiently appearing peak. The spectral shift of this peak is further displayed in Fig. 2b. The shift is about 8 cm⁻¹,

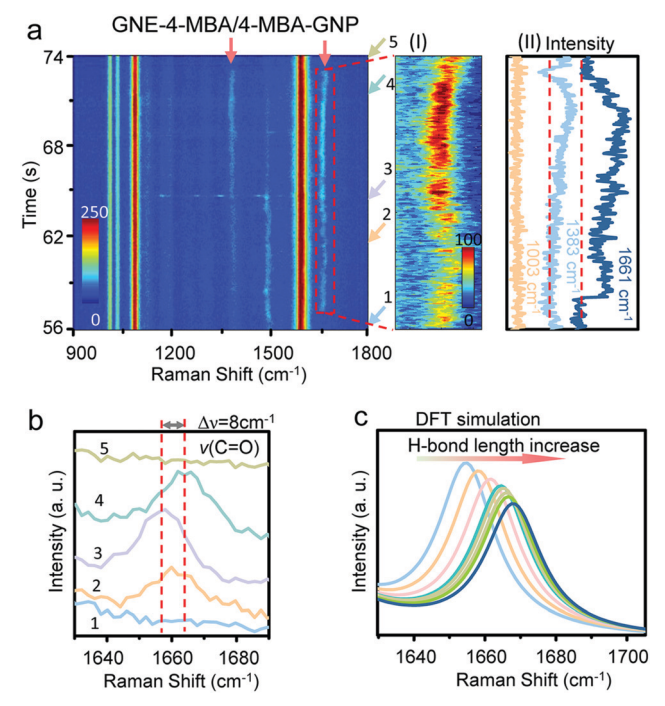


Fig. 2 Spectral changes in established GNE-4-MBA/4-MBA-GNP junctions. (a) Representative SERS time trajectory of GNE-4-MBA/4-MBA-GNP junction showing sudden appearance of both $\nu(COO^-)$ and $\nu(C=O)$ modes. (i) The zoom-in trajectory near the $\nu(C=O)$ mode. (ii) The intensity-time traces at 1003 cm⁻¹, 1383 cm⁻¹ and 1661 cm⁻¹. (b) Five selected spectra (indicated by the arrows in (a)) displayed with offset to show the spectral shifts of the ν (C=O) mode. (c) DFT simulation results of the blue-shift of ν (C=O) mode peak position with the increase of hydrogen bond length for the gold-4-MBA/4-MBA-gold junction. All the experiments were conducted at zero bias and the electrolyte containing no GNPs.

which is bigger than our spectral resolution 2 cm⁻¹. Another new peak appears around 1383 cm⁻¹. The inset (II) at the right ride shows the intensity-time traces at 1003 cm⁻¹, 1383 cm⁻¹ and 1661 cm⁻¹. The trace of 1003 cm⁻¹ is very stable. In contrast, there is a sudden jump of intensity of 1661 cm⁻¹ at 57 s. The peak at 1383 cm⁻¹ does not appear abruptly with the 1661 cm⁻¹ peak at 57 s but increases gradually afterwards. Because all major 4-MBA peaks and the background are stable, no movement of adsorbed GNP is involved and the established molecular junction should remain stable during the dynamic change of both new peaks.

Both new peaks have never been observed in one-molecule junctions containing only 4-MBA under similar conditions at neutral pH. Therefore, the interaction between carboxyl groups and gold atoms cannot produce both vibrational bands. Because both peaks only appear after the stable appearance of 1003 cm⁻¹ and 1027 cm⁻¹ peaks, we attribute the origin of both new peaks to the formation of additional h-bonds between two carboxyl groups, which have higher binding energy and shorter bond distance than the already existing non-specific intermolecular interactions. Considering the lower surface coverage of 4-MBA on the GNE apex, the estimated 4-MBA number in the 'hotspot' of the GNP-molecule-GNE structure is less than 46 molecules (see ESI,† S1). It is expected that the chance to form h-bonds between limited numbers of molecules at a certain time is low. The steady Raman signal is from all the 40-50 molecules in the 'hotspot'. However, the stochastic and abrupt changes of two new peaks are likely at the singlemolecule level.

DFT calculations (see Fig. S1, ESI†) of h-bonded 4-MBA/ 4-MBA pair suggest that the formation of h-bonds will induce the appearance of the stretching mode of C=O (ν (C=O)) near 1661 cm⁻¹. With the formation of stronger h-bonds between two carboxyl groups, the distance between two groups in the junction is further reduced. The proton of one carboxyl group moves closer to the oxygen atom of C=O of the opposite carboxyl group. The dislocation of the proton deforms the electron cloud of C=O, resulting in the ν (C=O) mode with reduced energy in Raman. The peak at 1383 cm⁻¹ is attributed to the vibrational modes $\nu(COO^-)$ of the carboxyl group. The $\nu(COO^{-})$ peak of 4-MBA appears when the -COOH group is deprotonated (see Fig. S7b, ESI†) or binds with divalent metal ions like Cu²⁺. Here, the h-bonds between two 4-MBA molecules push the proton away from the oxygen atom of -OH in one carboxyl group, and towards the C=O of the opposite carboxyl group, which promotes the $\nu(COO^-)$ mode. It is interesting to note that the formation of h-bonds enhances both $\nu(C=O)$ and $\nu(COO^-)$ modes. In contrast, only one mode is enhanced in pH experiments (see Fig. S7b, ESI†). Fig. S6 (ESI†) also shows the results from the established GNE-4-ATP/4-MBA-GNP junction. Different from the 4-MBA/4-MBA junction, only the peak of ν (C=O) can be transiently observed.

Previous STM experiments have also demonstrated the formation of two symmetric h-bonds between two 4-MBA molecules.³⁶ It has also been demonstrated before by different spectroscopic methods that asymmetric h-bonding can occur

between the primary amine and carboxyl groups. 23,37 Based on DFT calculations, the relative total strength of two symmetric h-bonds formed between two 4-MBA molecules is stronger than that of two asymmetric h-bonds formed between 4-ATP and 4-MBA (see Scheme 1 and Fig. S2, ESI†). The formation of stronger h-bonds likely leads to increased proton delocalization, charge transfer and charge redistributions, resulting in the appearance of both peaks of $\nu(COO^-)$ and $\nu(C=O)$ modes in 4-MBA/4-MBA junctions. In addition, the ν (C=O) peak of the 4-MBA/4-MBA pair junction appears more often and with a longer 'on' time for each appearance in general. These differences support that stronger h-bonds can be formed between two carboxyl groups than between carboxyl and amine groups. The results of DFT calculations also reveal that the strength of C=O is strongly affected by the strength of h-bonding. As shown in Fig. 2c, with the increase of h-bond length (or the decrease of h-bond strength) between two 4-MBA molecules, the frequency of the $\nu(C=0)$ mode blue-shifts, indicating the increased C=0 bond strength. Therefore, the spectral shifts in Fig. 2a(I) and b reveal the dynamic change of h-bond strength. It is also noted that the observed lifetime of the h-bonds in both molecule-pair junctions is quite long (often >10 s). This can be attributed to the improved stability of h-bonds confined in a nanocavity. A similar time scale of h-bond lifetime has been observed in the molecular junctions formed by STM.³⁸ It is also important to note that the formed h-bond may break and reform transiently at a fast rate during the over 10 s on time. Such fast dynamics are averaged out in the recorded SERS signal with a time resolution of 50 ms.

Electromechanical modulation of intermolecular interactions in molecule-pair junctions

It has been demonstrated that the electric force generated by the applied bias on the GNE could mechanically modulate the gap distance between the adsorbed GNP with charge and the gold substrate while the system is in the electrolyte. 39-41 A positive (negative) bias can push (pull) the negatively charged GNP towards (away from) the GNE surface. Along with the GNP movement, the attached molecule-pair can be mechanically compressed or stretched. The intermolecular interactions are expected to be affected most because they are the weakest link in the molecule-pair junction.

Here, we employ the electromechanical modulation method in the established 4-MBA/4-MBA pair junction. To avoid unwanted electrochemical reactions, the applied bias range is limited between -0.5 V and +0.5 V. It should be noted that the 4-MBA is chemically stable in the applied potential range. We first discuss the voltage-dependent change of the intensity of 7a (I_{7a}) . The 7a mode is spatially away from the head group and is therefore less affected by the carboxyl group-involved interfacial interactions. Therefore, the change of I_{7a} better reflects the gap distance change. To compare the change of I_{7a} between different junctions, we used normalized $I_{7a} = I_{7a} (V)/I_{7a} (0 V)$, where $I_{7a} (0 V)$ is the value at zero bias. As shown in Fig. 3a, the normalized I_{7a} of the 4-MBA/4-MBA molecule-pair junction (blue colored plot) increases at positive bias and decreases at negative bias. These changes are much bigger compared with the changes (red colored plot) of the 4-MBA one-molecule junction. For each

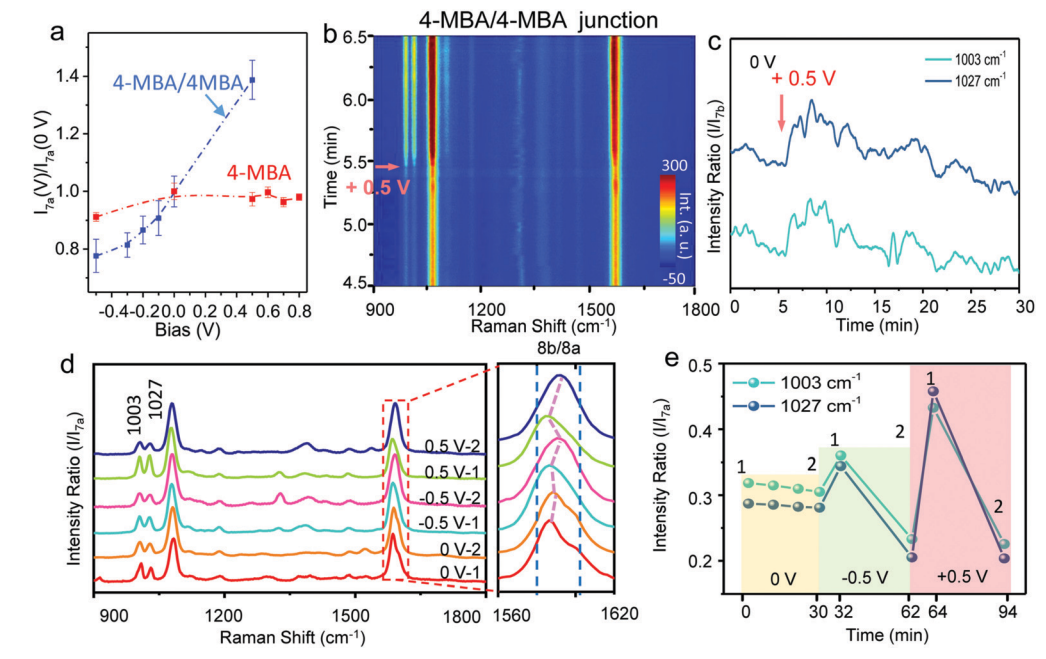


Fig. 3 Electromechanical modulation of GNE-4-MBA/4-MBA-GNP junctions. (a) Normalized I_{7a} changes at different biases for 4-MBA/4-MBA molecule-pair and 4-MBA one-molecule junctions. The dashed lines are to guide the eye. (b) A time-resolved SERS trajectory to show the intensity and spectral changes after applying $+0.5\,\text{V}$. (c) The time traces of intensity ratio (/// I_{7a} , I is normalized to I_{7a} at the same bias) for modes at 1003 cm $^{-1}$ and 1027 cm⁻¹. (d) Six stacked spectra to show the spectral changes at the beginning (1) and the end (2) of a half-hour duration of each bias application. The zoom-in spectra of mode 8b/8a peak are shown at the right. (e) The intensity ratio changes of two modes at 1003 cm⁻¹ and 1027 cm⁻¹ induced by three sequentially applied biases, each for half an hour.

Paper

pair junctions.

point in Fig. 3a, we apply the constant bias for half an hour so the bias-induced spectral change is fully stabilized. These changes can be explained by the electromagnetic (EM) enhancement mechanism and the intensity increases when the gap distance decreases. We speculate that the bigger bias-induced I_{7a} intensity change of 4-MBA/4-MBA molecule-pair junctions reveals the bigger compressibility of the molecule-

When a positive bias (+0.5 V) is applied to an established 4-MBA/4-MBA junction, we observe an instant intensity increase of all the vibration peaks (Fig. 3b) due to the EM enhancement mechanism. Furthermore, the intensity ratio I/I_{7a} (V) of 1003 cm⁻¹ and 1027 cm⁻¹ peaks increases immediately after applying +0.5 V (Fig. 3c). The additional increase of both modes suggests the enhancement of intermolecular interactions right after applying +0.5 V. In contrast, we did not observe the instant increase in the 4-MBA one-molecule junction (see Fig. S7c and d, ESI†). Therefore, the application of positive bias can immediately improve the intermolecular interactions of the relatively more compressible 4-MBA/4MBA junction. The different spectral responses to bias can also help to distinguish the interactions of carboxyl-carboxyl from gold-carboxyl. The no-response from the 4-MBA one-molecule junction also suggests that the lateral intermolecular interactions from neighbouring molecules²³ do not play important roles during the bias application.

To further confirm the above speculation, instead of applying positive bias, we firstly apply -0.5 V to the 4-MBA/4-MBA junction to stretch the junction. As shown in the zoom-in spectra at the right side of Fig. 3d, no instantaneous change is observed right after applying -0.5 V (cyan colored spectrum). However, after applying -0.5 V for half an hour, the 8b/8a peak blue-shifts towards the position of 8a (pink colored spectrum), indicating weakened interactions due to junction elongation. We then apply +0.5 V to compress the junction, as expected, the 8b/8a peak red-shifts rather quickly towards 8b. However, after applying +0.5 V continuously for half an hour, the 8b/8a peak blue-shifts back towards symmetric 8a. This back-and-forth shift of 8b/8a peak position with a magnitude about 8 cm⁻¹ under continuous positive bias application can be attributed to the continuous junction compression, which leads to a favorable configuration initially but an unfavorable configuration later. Similar responses are also observed in the intensity changes of 1003 cm⁻¹ and 1027 cm⁻¹ peaks. As shown in Fig. 3e, after applying -0.5 V, the intensity ratio (I/I_{7a}) slightly increases ($\sim 20\%$) initially (1), then slowly decreases to a much lower value (\sim 33% of initial value) in half an hour (2). During the sequential application of +0.5 V bias, the same fast increase-slow decrease pattern is observed but the spectral change is more dramatic (~125% change). The intriguing back-and-forth spectral changes of three b2 modes of 4-MBA under both negative and positive biases demonstrate that the intermolecular interactions in the 4-MBA/4-MBA junction are sensitive to the gentle mechanical perturbation by bias application. The optimal gap distance can only be transiently reached shortly after either applying negative or positive biases. Prolonged

application of both negative and positive biases leads to unfavorable gap distances for intermolecular interactions in the 4-MBA/4-MBA junction. However, although the gap distance varies, both peaks at 1003 and 1027 cm⁻¹ of these established junctions never fully disappear. Therefore, the intermolecular interactions can survive the extra electrical force and keep the adsorbed GNPs from being removed from the GNE surface.

Electromechanical modulation of intermolecular H-bonds in molecule-pair junctions

Now we investigate the effect of mechanical modulation to the transiently formed h-bonds in the established 4-MBA/4-MBA molecule-pair junction by monitoring bias-dependent SERS changes of both $\nu(COO^-)$ and $\nu(C=O)$ modes of the 4-MBA molecule. As we discussed earlier, both $\nu(COO^-)$ and $\nu(C=O)$ modes only appear upon the formation of h-bonds between two carboxyl groups. We notice that both modes are obviously affected by the applied bias. At zero bias, both modes appear stochastically all the time. However, the $\nu(COO^-)$ mode does not show up at all at negative biases and the $\nu(C=O)$ mode becomes fully silent after prolonged application of either positive or negative biases. Under negative biases, the time of the last appearance of the $\nu(C=O)$ mode peak in Raman spectra decreases with the increase of the magnitude of the negative bias (see Fig. S8, ESI†). These phenomena are consistent with the bias-dependent change of the asymmetric vibrational modes of 4-MBA we discussed earlier. However, the stronger h-bond is more sensitive to the bias induced gap distance change and can only be formed within a limited range of gap distance. The longer bias application time prevents the formation of h-bonds due to the larger deviation from the favored gap distance, presumably close to the total length of two 4-MBA molecules (~1.8 nm) in head-to-head configuration. In contrast, the peaks at 1003 cm⁻¹ and 1027 cm⁻¹ show up most of the time at different biases although the peak height varies. Therefore, the non-specific intermolecular interactions can survive a larger distortion in interaction distance than the intermolecular h-bond.

We compare the mean 'on' time $(\langle T_{on} \rangle)$ of the transiently appearing $\nu(C=0)$ mode in the trajectories at different biases. In the experiment, we first apply a non-zero bias for 35 minutes, and then return to zero bias for 30 minutes to relax the junction before applying another bias. The $\langle T_{on} \rangle$ of the $\nu(C=O)$ mode, reflecting the average lifetime of h-bonds, is shown in Fig. 4a. The representative SERS trajectories in a heat map and the intensity-time traces are shown in Fig. 4b. The intensity-time traces of $\nu(C=O)$ and $\nu(COO^-)$ modes are plotted as navy blue and light blue lines, respectively. With the application of pulling force to the molecule-pair junction, both the chance to form h-bonds and the stability of the formed h-bonds in the stretched junction are expected to be lower. Indeed, the $\langle t_{\rm on} \rangle$ is obviously reduced with the increase of the magnitude of negative bias. For example, the mean lifetime at -0.2 V is only about 10% of that at zero bias. No $\nu(C=O)$ mode appeared anymore beyond -0.3 V. In contrast, the $\langle t_{\rm on} \rangle$ of $\nu(C=0)$ is about 5 times longer at +0.5 V than that at zero bias.

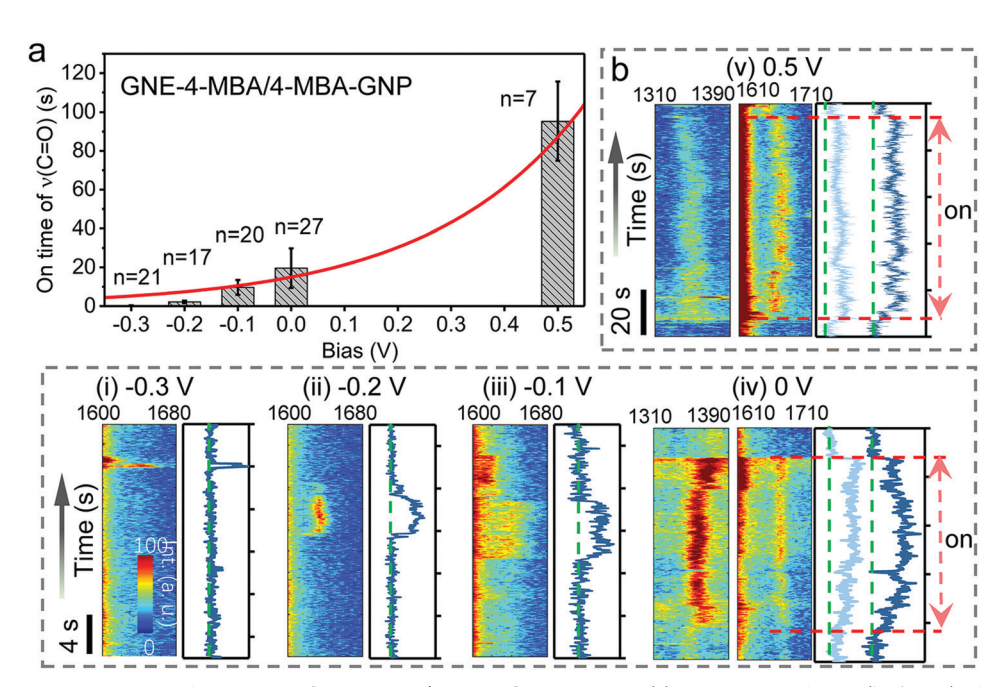


Fig. 4 Electromechanical modulation of h-bonds in GNE-4-MBA/4-MBA-GNP junctions. (a) The average lifetime ('on' time) of the ν (C=O) peak as a function of applied bias. To be consistent, only data appearing in the first 30 minutes are analyzed. Error bars are the standard deviation of n events. The red curve is a fitting curve based on (b). The representative time-resolved SERS trajectories in a heat map of the ν (C=O) mode at applied bias -0.3 V (i), -0.2 V (ii), and -0.1 V (iii), and of both ν (COO⁻) and ν (C=O) modes at zero bias (iv) and +0.5 V (v). The corresponding intensity-time traces of the ν (COO⁻) mode (light blue color) are shown at the right side of each SERS time trajectory. In (iv) and (v), the intensity-time traces of the ν (COO⁻) mode (light blue color) are also shown. The green dashed lines indicate the baselines at the 'off' state.

Therefore, once the h-bonds are formed at the 4-MBA/4-MBA interface, they become very stable in a compressed junction. The nano confinement effect should contribute to the long-lived h-bonds between two 4-MBA molecules at +0.5 V. Assuming that the modulating force is an effective electric force proportional to bias V, we can fit the $\langle t_{\rm on} \rangle$ -bias data in Fig. 4a using the Arrhenius equation $\langle t_{\rm on} \, V \rangle = \langle t_{\rm on} \, (0 \, V) e^{qV/k_{\rm B}T} \rangle$, where q is a fitting parameter for effective charge, $k_{\rm B}$ is the Boltzmann constant and T is room temperature. The data can be fitted reasonably well with $\langle t_{\rm on} \, (0 \, V) \rangle = 15 \, {\rm s}$ and q = 0.091e (e is the electron charge). We notice that the measured lifetime dropped faster at negative biases. One reason is likely to be due to the proton reduction at the GNE and GNP surfaces at negative biases, which further reduces the lifetime of h-bonds. 42

Conclusions

In summary, we have successfully probed the dynamic development of intermolecular interactions during the formation of molecule-pair junctions driven by individual GNP collision events on the GNE. Characteristic Raman vibrational modes of 4-MBA, mainly associated with the carboxyl group, are identified and used to differentiate h-bonds from non-specific intermolecular interactions. Utilizing these fingerprint modes, we find that the non-specific intermolecular interactions are mainly responsible for the retention of GNP on the GNE. The intermolecular interactions are too weak to be detected during transient 'hit-stay-run' events but can gradually develop in

'hit-n-stay' events to retain the GNP on the GNE surface. After the immobilization of the GNP by non-specific intermolecular interactions, intermolecular h-bonds can be formed in the established junctions. These h-bonds only appear for a short time (on the order of 10 s) and the appearance is stochastic. For comparison, we constructed both hetero- and homo-molecular pairs in the plasmonic junction. As expected, stronger hydrogen bonds, inducing longer time and bigger Raman changes, appeared at the symmetric carboxyl/carboxyl interface rather than at the asymmetric carboxyl/amine interface. We further demonstrated that the applied biases on the GNE could slowly alter the gap distance, leading to a gentle mechanical modulation of intermolecular interactions in the established moleculepair junctions. We also investigated how the stability of h-bonds were affected by the electromechanical modulation and found the h-bonds were more sensitive to the modulation.

The detailed studies of various intermolecular interactions during and after the single GNP collisions will provide insights for the development of electrochemical 'nano-impact' technique based biosensors. The 'hit-stay-run' and 'hit-n-stay' collision events to some extent mimic the break-junction and fixed-junction methods often used in single-molecule conductance measurements. Therefore, these SERS studies can also improve the molecular level understanding of the recognition tunneling technique. In biology, the reversible intermolecular interactions between carboxyl and amine groups are ubiquitous and often happen in confined spaces with a locally controllable environment. Here the two interacting molecules are confined in a nanometer gap between two gold nanostructures, with

PCCP Paper

adjustable environmental parameters. This technique has the potential to study the detailed dynamics of various intermolecular interactions and chemical reactions in a confined space with millisecond time resolution.

Experimental

Chemicals

4-MBA and 4-ATP were purchased from Sigma-Aldrich. Phosphate buffered saline (PBS) powder (pH 7.3-7.5) and absolute ethanol (200 proof) were purchased from Fisher Scientific. Potassium ferrocyanide (K₄[Fe(CN)₆]), 98.5% purity, analysis grade was purchased from Acros Organics. Citrate stabilized 40 nm diameter GNPs were purchased from Ted Pella, Inc. All the chemicals were used directly without further purification. All the aqueous solutions were prepared using deionized water by a Purelab system from ELGA/Siemens.

Chemical modification of GNE and GNP

The details of electrochemical etching, insulation, and characterization of GNE can be found in previous works. 22,47 The cleaned GNEs are immersed in model molecule (5 mM for 4-ATP and 50 mM for 4-MBA) ethanol solutions for at least 7 h to achieve a high quality SAM at the GNE apex. The surface coverage of 4-MBA on the GNE apex is evaluated by cyclic voltammograms (CVs) (see Fig. S1, ESI†).

150 pM citrate-stabilized GNPs are functionalized with 70 μM 4-MBA to ensure a full surface coverage. After incubating overnight at room temperature, the 4-MBA-GNP solution is centrifuged (at a speed of 5000 rpm for 10 minutes) and rinsed 3 times to remove the excess 4-MBA in the solution.

Measurements

SERS is performed on a home-built Raman microscopy setup based on a Nikon Ti-U microscope. 13 Briefly, a 632.8 nm laser beam is focused by a $40 \times$ objective lens at the apex of a partially insulated GNE that is placed in a liquid cell installed on the microscope sample stage. The time-resolved SERS trajectories are collected with a time resolution of 50 ms by a CCD camera (PIXIS 100B_eXcelon, Princeton Instrument). The spectral resolution is about 2 cm⁻¹.

The EC current is amplified by an Axon 200B patch clamp amplifier (Molecular Devices Inc., CA) in voltage clamp mode and recorded at a 50 kHz sampling rate by an Axon Digidata 1440A (Molecular Devices Inc., CA). The Axon setup is synchronized by the trigger signal sent from the CCD camera. The GNE is used as the working electrode and the Ag/AgCl wire electrode is used as the quasi-reference electrode. All the measurements are performed at room temperature in electrolyte. The typical electrolyte is 5 mM PBS (pH 7.4) containing 3 mM potassium ferrocyanide. We also use 10 mM PBS without ferrocyanide ions for some experiments and no noticeable difference is observed in the SERS signal. The typical concentration of GNP is 30 pM for the 'hit-stay-run' experiments and no GNPs are added when

investigating the established molecular junction under adsorbed GNPs on the GNE.

Raman spectra calculation

The optimized geometry and Raman spectra of gold-molecule complexes-gold junctions are obtained with density functional theory (DFT) calculations (see Fig. S2, ESI†). The structures are geometrically optimized using the B3LYP exchange-correlation functional and 6-31+G* basis set for molecules and LANL2DZ basis set for gold atoms. To vary the h-bond length of hydrogenbonded two-molecule complexes, we set the distance between two fixed gold atoms at different values. The calculated Raman spectra are plotted by applying a Lorentzian function with a full-width at half-height (FWHH) of 20 cm⁻¹. A scaling factor of 0.965 is applied for all the modes.

Conflicts of interest

There are no conflicts to declare.

Acknowledgements

This work is partially supported by the Engineering Research Centers Program of the National Science Foundation under NSF Cooperative Agreement No. EEC-1647837, NSFC (21673023, 21705122, and 21372183), and the Program for Innovative Teams of Outstanding Young and Middle-aged Researchers in the Higher Education Institutions of Hubei Province (T201702). S. C. also acknowledges the financial support from the Thousand Youth Talents Program of China. T. M. acknowledges the support from the graduate student study abroad program, and the postgraduate and college student innovation and entrepreneurship training program of WUST. We acknowledge the computing resources provided by the Instructional & Research Computing Center (IRCC) at Florida International University.

Notes and references

- 1 C. Bissantz, B. Kuhn and M. Stahl, J. Med. Chem., 2010, 53, 5061-5084.
- 2 L. Bartels, Nat. Chem., 2010, 2, 87.
- 3 C. Heinzmann, C. Weder and L. M. de Espinosa, Chem. Soc. Rev., 2016, 45, 342-358.
- 4 B. A. Mantooth and P. S. Weiss, Proc. IEEE, 2003, 91, 1785-1802.
- 5 C.-a. Di, G. Yu, Y. Liu and D. Zhu, J. Phys. Chem. B, 2007, 111, 14083-14096
- 6 H. Bayley and P. S. Cremer, Nature, 2001, 413, 226-230.
- 7 R. Wei, V. Gatterdam, R. Wieneke, R. Tampé and U. Rant, Nat. Nanotechnol., 2012, 7, 257.
- 8 S. Senapati and S. Lindsay, Acc. Chem. Res., 2016, 49, 503-510.
- 9 O. Takahito and U. Yoshio, Proc. Natl. Acad. Sci. U. S. A., 2006, 103, 10-14.

- 10 S. Lindsay, J. He, O. Sankey, P. Hapala, P. Jelinek, P. Zhang, S. Chang and S. Huang, *Nanotechnology*, 2010, 21, 262001.
- 11 C. Zhou, X. Li, Z. Gong, C. Jia, Y. Lin, C. Gu, G. He, Y. Zhong, J. Yang and X. Guo, *Nat. Commun.*, 2018, **9**, 807.
- 12 Y. Zhao, B. Ashcroft, P. Zhang, H. Liu, S. Sen, W. Song, J. Im, B. Gyarfas, S. Manna, S. Biswas, C. Borges and S. Lindsay, *Nat. Nanotechnol.*, 2014, **9**, 466–473.
- 13 S. Huang, J. He, S. Chang, P. Zhang, F. Liang, S. Li, M. Tuchband, A. Fuhrmann, R. Ros and S. Lindsay, *Nat. Nanotechnol.*, 2010, 5, 868–873.
- 14 J. Im, S. Sen, S. Lindsay and P. Zhang, ACS Nano, 2018, 12, 7067–7075.
- 15 J. Im, S. Biswas, H. Liu, Y. Zhao, S. Sen, S. Biswas, B. Ashcroft, C. Borges, X. Wang, S. Lindsay and P. Zhang, *Nat. Commun.*, 2016, 7, 13868.
- 16 A. B. Zrimsek, N. Chiang, M. Mattei, S. Zaleski, M. O. McAnally, C. T. Chapman, A. I. Henry, G. C. Schatz and R. P. Van Duyne, *Chem. Rev.*, 2017, 117, 7583–7613.
- 17 H.-K. Choi, W.-H. Park, C.-G. Park, H.-H. Shin, K. S. Lee and Z. H. Kim, *J. Am. Chem. Soc.*, 2016, **138**, 4673–4684.
- 18 E. A. Sprague-Klein, B. Negru, L. R. Madison, S. C. Coste, B. K. Rugg, A. M. Felts, M. O. McAnally, M. Banik, V. A. Apkarian, M. R. Wasielewski, M. A. Ratner, T. Seideman, G. C. Schatz and R. P. Van Duyne, *J. Am. Chem. Soc.*, 2018, 140, 10583–10592.
- 19 Z. Liu, S.-Y. Ding, Z.-B. Chen, X. Wang, J.-H. Tian, J. R. Anema, X.-S. Zhou, D.-Y. Wu, B.-W. Mao, X. Xu, B. Ren and Z.-Q. Tian, *Nat. Commun.*, 2011, 2, 305.
- 20 W. Xi, B. K. Shrestha and A. J. Haes, *Anal. Chem.*, 2018, **90**, 128–143.
- 21 P. Martin, ACS Nano, 2014, 8, 7555.
- 22 J. Guo, J. Pan, S. Chang, X. Wang, N. Kong, W. Yang and J. He, *Small*, 2018, **14**, e1704164.
- 23 H. T. Phan and A. J. Haes, J. Phys. Chem. C, 2018, 122, 14846–14856.
- 24 F. Wang, R. G. Widejko, Z. Yang, K. T. Nguyen, H. Chen, L. P. Fernando, K. A. Christensen and J. N. Anker, *Anal. Chem.*, 2012, 84, 8013–8019.
- 25 S. J. Lee and M. Moskovits, Nano Lett., 2011, 11, 145-150.
- 26 Y. F. Huang, H. P. Zhu, G. K. Liu, D. Y. Wu, B. Ren and Z. Q. Tian, J. Am. Chem. Soc., 2010, 132, 9244–9246.
- 27 D. Y. Wu, J. F. Li, B. Ren and Z. Q. Tian, *Chem. Soc. Rev.*, 2008, 37, 1025–1041.
- 28 G. Di Martino, V. A. Turek, A. Lombardi, I. Szabo, B. de Nijs, A. Kuhn, E. Rosta and J. J. Baumberg, *Nano Lett.*, 2017, 17, 4840–4845.

- 29 P. C. Sevinc, B. Dhital, V. G. Rao, Y. Wang and H. P. Lu, I. Am. Chem. Soc., 2016, 138, 1536–1542.
- 30 S. M. Oja, D. A. Robinson, N. J. Vitti, M. A. Edwards, Y. Liu, H. S. White and B. Zhang, J. Am. Chem. Soc., 2017, 139, 708-718
- 31 I. Chakraborty, A. Som, T. Adit Maark, B. Mondal, D. Sarkar and T. Pradeep, *J. Phys. Chem. C*, 2016, **120**, 15471–15479.
- 32 A. Michota and J. Bukowska, J. Raman Spectrosc., 2003, 34, 21–25.
- 33 X. Zhang, Z. Yu, W. Ji, H. Sui, Q. Cong, X. Wang and B. Zhao, J. Phys. Chem. C, 2015, 119, 22439–22444.
- 34 Y. Wang, W. Ji, H. Sui, Y. Kitahama, W. Ruan, Y. Ozaki and B. Zhao, J. Phys. Chem. C, 2014, 118, 10191–10197.
- 35 L. Guerrini, E. Pazos, C. Penas, M. E. Vázquez, J. L. Mascareñas and R. A. Alvarez-Puebla, J. Am. Chem. Soc., 2013, 135, 10314–10317.
- 36 T. Nishino, N. Hayashi and P. T. Bui, J. Am. Chem. Soc., 2013, 135, 4592–4595.
- 37 G. Kladnik, M. Puppin, M. Coreno, M. de Simone, L. Floreano, A. Verdini, A. Morgante, D. Cvetko and A. Cossaro, *Nano Lett.*, 2016, 16, 1955–1959.
- 38 S. Huang, J. He, S. Chang, P. Zhang, F. Liang, S. Li, M. Tuchband, A. Fuhrman, R. Ros and S. Lindsay, *Nat. Nanotechnol.*, 2010, 5, 868–873.
- 39 X. Shan, Y. Fang, S. Wang, Y. Guan, H. Y. Chen and N. Tao, Nano Lett., 2014, 14, 4151–4157.
- 40 N. Farnaz, A. I. Wang, E. M. Sletten, S. Yi, K. Jing, Y. Eli, T. M. Swager, J. H. Lang and B. Vladimir, *ACS Nano*, 2015, 9, 7886–7894.
- 41 Y. Wang and G. Zocchi, Phys. Rev. Lett., 2010, 105, 238104.
- 42 G. Di Martino, V. A. Turek, A. Lombardi, I. Szabó, B. de Nijs, A. Kuhn, E. Rosta and J. J. Baumberg, *Nano Lett.*, 2017, 17, 4840–4845.
- 43 S. J. Kwon and A. J. Bard, *J. Am. Chem. Soc.*, 2012, **134**, 10777–10779.
- 44 A. D. Castaneda, N. J. Brenes, A. Kondajji and R. M. Crooks, J. Am. Chem. Soc., 2017, 139, 7657–7664.
- 45 J. E. Dick, A. T. Hilterbrand, A. Boika, J. W. Upton and A. J. Bard, *Proc. Natl. Acad. Sci. U. S. A.*, 2015, **112**, 5303–5308.
- 46 F. Chen, J. Hihath, Z. Huang, X. Li and N. J. Tao, Annu. Rev. Phys. Chem., 2007, 58, 535–564.
- 47 M. Tuchband, J. He, S. Huang and S. Lindsay, *Rev. Sci. Instrum.*, 2012, **83**, 015102.